J|A|C|S COMMUNICATIONS

Published on Web 09/14/2010

A Bifunctional Nonprecious Metal Catalyst for Oxygen Reduction and Water Oxidation

Yelena Gorlin and Thomas F. Jaramillo*

Department of Chemical Engineering, Stanford University, Stanford, California 94305-5025

Received May 28, 2010; E-mail: jaramillo@stanford.edu

Abstract: There is a growing interest in oxygen electrochemistry as conversions between O_2 and H_2O play an important role in a variety of renewable energy technologies. The goal of this work is to develop active bifunctional catalyst materials for water oxidation and oxygen reduction. Drawing inspiration from a cubane-like $CaMn_4O_x$, the biological catalyst found in the oxygen evolving center (OEC) in photosystem II, nanostructured manganese oxide surfaces were investigated for these reactions. Thin films of nanostructured manganese oxide were found to be active for both oxygen reduction and water oxidation, with similar overall oxygen electrode activity to the best known precious metal nanoparticle catalysts: platinum, ruthenium, and iridium. Physical and chemical characterization of the nanostructured Mn oxide bifunctional catalyst reveals an oxidation state of Mn(III), akin to one of the most commonly observed Mn oxidation states found in the OEC.

There is a growing interest in oxygen electrochemistry as conversions between O_2 and H_2O play important roles in renewable energy technologies. The oxygen reduction reaction (ORR) is the ubiquitous cathode reaction in fuel cells, while the oxygen evolution reaction (OER) is the anode reaction employed in electrolysis cells; the OER may also serve to balance solar fuel synthesis reactions, e.g. CO_2 reduction to fuels. A bifunctional catalyst for both reactions could be employed in a unitized regenerative fuel cell (URFC), an energy storage device that can be coupled to intermittent renewable energy such as wind or solar to peak-shift electricity to the grid.[1] Catalyst development is critical in these fields. The best catalysts for the ORR consist of platinum (Pt),[2] but Pt has only moderate activity for the OER.[3] Ruthenium (Ru) and iridium (Ir) oxides are the best OER catalysts,[3] but they are not as active for the ORR as Pt.[4] Alloys of Pt, Ir, and Ru have consequently been evaluated for bifunctional oxygen electrode activity, and they were shown to perform better than the pure metals or metal oxides.[1,5] Nevertheless, bifunctional catalyst development remains a major challenge as the best catalysts require significant overpotentials for both reactions and consist of precious metals that are both scarce and expensive.

In nature, the OER is catalyzed by the oxygen evolving complex (OEC) with a cubane-like $CaMn_4O_x$ active site.[6] Density functional theory (DFT) calculations have helped explain the high activity: each step in the reaction is close to thermoneutral, a requirement for a reversible catalyst.[7] Thus, manganese (Mn) oxide surfaces and molecular mimics are potentially interesting materials for bifunctional oxygen catalysis. A number of Mn-based molecular mimics[8−10] and Mn oxide surfaces[11−14] have already demonstrated activity for the OER, particularly the alpha-Mn_2O_3 phase.[11] Though alpha-Mn_2O_3 has not previously shown activity for the ORR,[15] other Mn oxide phases are ORR active, particularly MnOOH,[15] beta-MnO_2,[16] and alpha-MnO_2.[17] Drawing inspiration from the nanoscaled $CaMn_4O_x$ active site of the OEC, we have developed an active Mn oxide bifunctional catalyst, a nanostructured thin film with such high activity in alkaline media that it nearly reaches that of the most active precious metals.

The Mn oxide thin film was electrodeposited potentiostatically onto a polished glassy carbon (GC) substrate in a three-electrode electrochemical cell in a rotating disk electrode configuration (RDE), using a modified literature procedure.[18] After deposition, the film was calcined at 480 °C in air for 10 h.

Electrochemical activity of the Mn oxide thin film was studied using cyclic voltammetry (CV) in a three-electrode electrochemical cell in an RDE configuration. CVs were measured in O_2-saturated 0.1 M KOH electrolyte at 23 °C and 1600 rpm, with a sweep rate of 5 $mV \cdot s^{-1}$, using a platinum wire counter electrode and Hg/HgO reference electrode. The potential scale was calibrated to a reversible hydrogen electrode (RHE). Further details are available in the Supporting Information. In order to benchmark the activity of the Mn oxide thin film, electrochemical characterization was also performed on commercial carbon-supported (Vulcan XC-72) precious metal nanoparticles: 20 wt % Pt (Etek), 20 wt % Ru (Premetek), and 20 wt % Ir (Premetek). Catalyst dispersions of Pt, Ir, and Ru nanoparticles were prepared using standard procedures for fuel cell catalyst testing[2] to achieve a metal concentration of 28 $\mu g \cdot cm^{-2}$ on a GC substrate. Measurements of the electrochemically active surface area (ECSA) showed that $ECSA_{MnOx} \leq ECSA_{precious\ metals}$ (see Supporting Information). A bare GC substrate, heat treated to 480 °C as with the Mn oxide sample, was examined as a control.

Catalytic activities for the ORR and the OER are shown in Figure 1, which exhibits their initial linear sweeps in an anodic direction. The Mn oxide thin film was found to be highly active for both the ORR and the OER. The Mn oxide thin film was more active for the ORR than both Ru and Ir nanoparticles and only ~130 mV less active than Pt at the half-wave potential. Regarding OER activity, the Mn oxide thin film was clearly more active than Pt with activity that approached those of Ir and Ru. As expected, the GC support itself showed little catalytic activity.

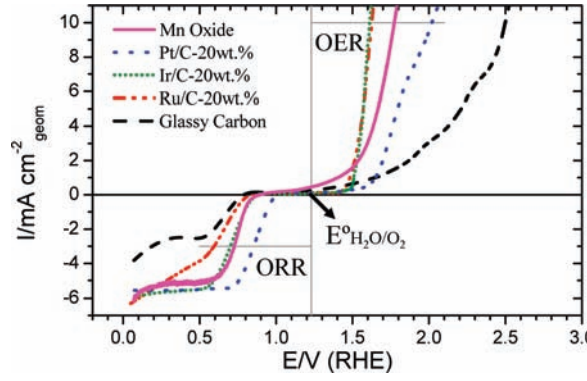

Figure 1. Oxygen electrode activities of the nanostructured Mn oxide thin film, nanoparticles of Pt, Ir, and Ru, and the GC substrate. The Mn oxide thin film shows excellent activity for both the ORR and the OER.

10.1021/ja104587v

Table 1 quantitatively compares the bifunctional oxygen electrode activity of the Mn oxide thin film to those of the precious metal nanoparticles. The figure of merit used to quantify ORR is the potential at which an ORR current density of 3 $mA \cdot cm^{-2}$ was reached, which approximates the half-wave potential. Activities for the OER were judged by the potential required to oxidize water at a current density of 10 $mA \cdot cm^{-2}$, a convention commonly used in the OER literature, and a metric relevant to solar fuel synthesis.[19] Two values are recorded for Pt nanoparticles as degradation of the carbon support complicates measurement of the potential needed for 10 $mA \cdot cm^{-2}$ on Pt (see the note below Table 1). To assess the overall oxygen electrode activity, the difference between the ORR and the OER metrics was tabulated. The smaller the difference, the closer the catalyst is to an ideal reversible oxygen electrode. By this metric, the nanostructured Mn oxide thin film has an oxygen electrode activity of 1.04 V, which compares favorably to the precious metal catalysts.

Table 1. Oxygen Electrode Activities

Catalyst Material	ORR: E(V) at $I = -3$ $mA \cdot cm^{-2}$	OER: E(V) at $I = 10$ $mA \cdot cm^{-2}$	Oxygen Electrode Δ(OER-ORR): E (V)
20 wt % Ir/C	0.69	1.61	0.92
20 wt % Ru/C	0.61	1.62	1.01
20 wt % Pt/C	0.86	2.02 (1.88)[a]	1.16 (1.02)[a]
Mn oxide	0.73	1.77	1.04

[a] Extrapolated value using the same Tafel slope as that at 1.74 V, where negligible corrosion occurs and the Pt is active for the OER.

To investigate the nature of this material's bifunctional activity, we employed X-ray diffraction (XRD), scanning electron microscopy (SEM), and X-ray photoelectron spectroscopy (XPS). XRD revealed some crystallinity, a weak peak at 32.9° consistent with alpha-Mn_2O_3(222); see Supporting Information. The fact that this material does not behave as previously reported alpha-Mn_2O_3 may be explained by the SEM images shown in Figure 2a and 2b, which exhibit a highly nanostructured surface with features that likely distinguish this surface from that of standard preparations.

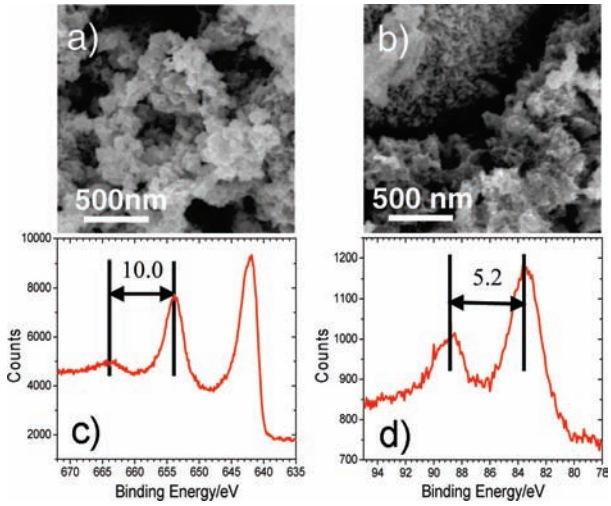

Figure 2. SEM images of the Mn oxide film in two locations: (a) and (b), revealing a nanostructured morphology. High resolution XPS spectra of Mn-2p and Mn-3s regions are shown in (c) and (d), respectively. The relative positions of the $2p_{1/2}$ satellite and the magnitude of 3s multiplet splitting were 10.0 and 5.2. These values indicate a Mn(III) oxide surface.

XPS was used to probe the Mn oxidation state at the surface, Figure 2c and 2d, by means of the relative position of the $2p_{1/2}$ satellite structure ($\Delta E2p_{1/2}$) and the magnitude of the 3s multiplet splitting ($\Delta E3s$). Powder standards of MnO, Mn_3O_4, Mn_2O_3, and MnO_2 were measured for comparison; see Supporting Information for details. Table 2 lists the measured values for the four standards along with previous measurements from literature.[20] For the active Mn oxide catalyst, $\Delta E2p_{1/2}$ and $\Delta E3s$ were 10.0 and 5.2, respectively, which correspond to Mn(III) in Mn_2O_3, the most common oxidation state in the OEC.[21]

This nanostructured Mn(III) oxide demonstrates bifunctional activity unlike other Mn oxides (see Supporting Information). Its OER activity is on par with the best reported Mn oxide OER catalyst,[12] while its ORR activity matches or surpasses the activities of the best reported Mn oxide ORR catalysts.[15−17] More importantly, its bifunctional activity is comparable to that of precious metals. Its OER activity also outperforms that of recently reported Co-based OER electrodes.[22] The excellent catalytic activity we observed likely stems from the nanostructured nature of the catalyst, which can facilitate the presence of the appropriate Mn_xO_y active sites at the relevant potentials to drive either the ORR or the OER. Further experimental and theoretical (DFT) studies are underway to understand the origins of this catalyst's bifunctional activity.

Table 2. XPS Values for Mn $\Delta E2p_{1/2}$ and Mn $\Delta E3s$ Splitting for Four Mn Oxide Standards, Obtained in This Work and from Ref 19

Sample	Source	$\Delta E2p_{1/2}$	$\Delta E3s$
MnO_2	this work	11.8	4.5
	ref 19	11.9	4.5
Mn_2O_3	this work	10.0	5.1
	ref 19	10.5	5.4
MnO	this work	6.0	6.0
	ref 19	5.4	6.1
Mn_3O_4	this work	10.5[a]	6.0[a]
	ref 19	11.3	5.3
Mn oxide catalyst in Figures 1 and 2		10.0	5.2

[a] A very broad peak is observed.

Inspired by nature's catalyst for water oxidation, we developed a thin-film analogue consisting of a nanostructured Mn(III) oxide. This inexpensive and earth-abundant catalyst exhibited excellent bifunctional oxygen electrode activity similar to that of the best known precious metal catalysts: Pt, Ru, and Ir. Such a catalyst could potentially be employed as the oxygen electrode in an alkaline exchange membrane (AEM) URFC[23] or AEM-PEM (proton exchange membrane) hybrid URFC.[24] This result opens up new avenues for energy conversion technologies based on earth-abundant, scalable, nonprecious metal catalysts.

Acknowledgment. The work was supported by the Global Climate and Energy Project (GCEP) and the U.S. Department of Energy, Office of Basic Energy Sciences as part of an Energy Frontier Research Center.

Supporting Information Available: Details on manganese oxide synthesis, XPS, SEM, XRD, electrochemical characterization, ECSA, a comparison to previously published ORR and OER catalysts, and a discussion on OER activity and solar fuel synthesis. This material is available free of charge via the Internet at http://pubs.acs.org.

References

(1) Chen, G. Y.; Bare, S. R.; Mallouk, T. E. *J. Electrochem. Soc.* **2002**, *149*, A1092.
(2) Gasteiger, H. A.; Kocha, S. S.; Sompalli, B.; Wagner, F. T. *Appl. Catal., B* **2005**, *56*, 9.
(3) Trasatti, S. *Electrochim. Acta* **1984**, *29*, 1503.
(4) Gnanamuthu, D. S.; Petrocelli, J. V. *J. Electrochem. Soc.* **1967**, *114*, 1036.
(5) Zhang, Y. J.; Wang, C.; Wan, N. F.; Mao, Z. Q. *Int. J. Hydrogen Energy* **2007**, *32*, 400.
(6) Ferreira, K. N.; Iverson, T. M.; Maghlaoui, K.; Barber, J.; Iwata, S. *Science* **2004**, *303*, 1831.

(7) Rossmeisl, J.; Dimitrievski, K.; Siegbahn, P.; Norskov, J. K. *J. Phys. Chem. C* **2007**, *111*, 18821.
(8) Brimblecombe, R.; Koo, A.; Dismukes, G. C.; Swiegers, G. F.; Spiccia, L. *J. Am. Chem. Soc.* **2010**, *132*, 2892.
(9) Limburg, J.; Vrettos, J. S.; Chen, H. Y.; de Paula, J. C.; Crabtree, R. H.; Brudvig, G. W. *J. Am. Chem. Soc.* **2001**, *123*, 423.
(10) Yagi, M.; Narita, K. *J. Am. Chem. Soc.* **2004**, *126*, 8084.
(11) Morita, M.; Iwakura, C.; Tamura, H. *Electrochim. Acta* **1979**, *24*, 357.
(12) Najafpour, M. M.; Ehrenberg, T.; Wiechen, M.; Kurz, P. *Angew. Chem., Int. Ed.* **2010**, *49*, 2233.
(13) Jiao, F.; Frei, H. *Chem. Commun.* **2010**, *46*, 2920.
(14) El-Deab, M. S.; Awad, M. I.; Mohammad, A. M.; Ohsaka, T. *Electrochem. Commun.* **2007**, *9*, 2082.
(15) Mao, L. Q.; Zhang, D.; Sotomura, T.; Nakatsu, K.; Koshiba, N.; Ohsaka, T. *Electrochim. Acta* **2003**, *48*, 1015.
(16) Lima, F. H. B.; Calegaro, M. L.; Ticianelli, E. A. *Electrochim. Acta* **2007**, *52*, 3732.
(17) Cheng, F. Y.; Su, Y.; Liang, J.; Tao, Z. L.; Chen, J. *Chem. Mater.* **2010**, *22*, 898.
(18) Tench, D.; Warren, L. F. *J. Electrochem. Soc.* **1983**, *130*, 869.
(19) Matsumoto, Y.; Sato, E. *Mater. Chem. Phys.* **1986**, *14*, 397. For a discussion on solar fuel synthesis, see Supporting Information.
(20) Dicastro, V.; Polzonetti, G. *J. Electron Spectrosc. Relat. Phenom.* **1989**, *48*, 117.
(21) Mukhopadhyay, S.; Mandal, S. K.; Bhaduri, S.; Armstrong, W. H. *Chem. Rev.* **2004**, *104*, 3981.
(22) Kanan, M. W.; Nocera, D. G. *Science* **2008**, *321*, 1072.
(23) Hickner, M. A. *Mater. Today* **2010**, *13*, 34.
(24) Unlu, M.; Zhou, J. F.; Kohl, P. A. *Angew. Chem., Int. Ed.* **2010**, *49*, 1299.

JA104587V